Taylor & Francis
Taylor & Francis Group

RESEARCH PAPER

Trypanosoma evansi evades host innate immunity by releasing extracellular vesicles to activate TLR2-AKT signaling pathway

Ran Wei, Xin Li, Xiaocen Wang, Nan Zhang, Yuru Wang, Xichen Zhang, Pengtao Gong[*], and Jianhua Li[*]

Key Laboratory of Zoonosis Research, Ministry of Education; College of Veterinary Medicine, Jilin University, Changchun, China

ABSTRACT

Surra, one of the most important animal diseases with economic consequences in Asia and South America, is caused by Trypanosoma evansi. However, the mechanism of immune evasion by T. evansi has not been extensively studied. In the present study, T. evansi extracellular vesicles (TeEVs) were characterized and the role of TeEVs in T. evansi infection were examined. The results showed that T. evansi and TeEVs could activate TLR2-AKT pathway to inhibit the secretions of IL-12p40, IL-6, and TNF-α in mouse BMDMs. TLR2$^{-/-}$ mice and mice with a blocked AKT pathway were more resistant to T. evansi infection than wild type (WT) mice, with a significantly lower infection rate, longer survival time and less parasite load, as well as an increased secretion level of IL-12p40 and IFN-γ. Kinetoplastid membrane protein-11 (KMP-11) of TeEVs could activate AKT pathway and inhibit the productions of IL-12p40, TNF-α, and IL-6 in vitro. TeEVs and KMP-11 could inhibit the productions of IL-12p40 and IFN-γ, promote T. evansi proliferation and shorten the survival time of infected mice in vivo. In conclusion, T. evansi could escape host immune response through inhibiting the productions of inflammatory cytokines via secreting TeEVs to activate TLR2-AKT pathway. KMP-11 in TeEVs was involved in promoting T. evansi infection.
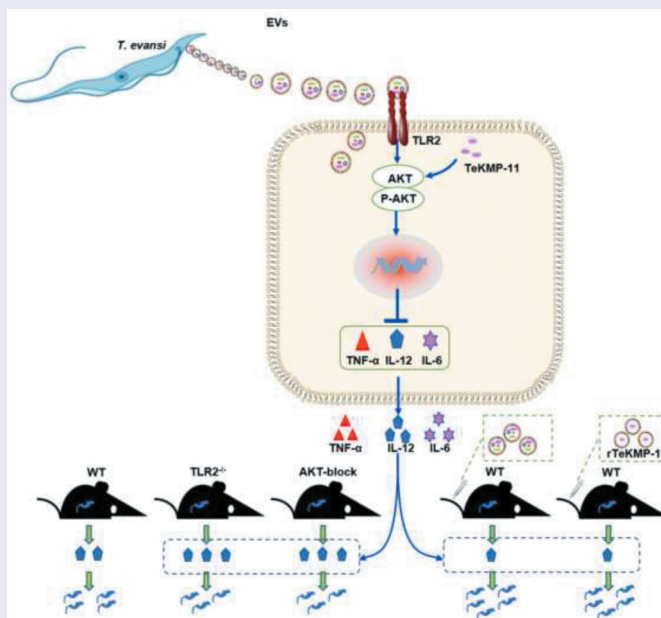
Extracellular vesicles (EVs) secreted by Trypanosoma evansi (T. evansi) activate the TLR2-AKT signaling pathway to inhibit the production of inflammatory cytokines, thereby escaping the host's immune response. Kinetoplastid membrane protein-11 (KMP-11) in EVs is related to the promotion of T.evansi infection via AKT pathway.

CONTACT Jianhua Li gong_pengtao@126.com; Pengtao Gong gong_pengtao@126.com
[*]These authors contributed equally.

 Supplemental data for this article can be accessed here

Introduction

Trypanosoma evansi is bloodborne protozoa that cause disease in several species and transmitted by hematophagous flies and vampire bats to cause surra, a serious disease of economic importance throughout the world [1]. *Trypanosoma evansi* could infect most mammals exhibiting different clinical characteristics [2,3]. In camels, horses, and dogs, the parasite causes acute infection causing high fever, weight loss, anemia, genital inflammation, neurological symptoms, and eventually death [4]. On the contrary, in cattle and buffalo, the parasite causes chronic infection and produces symptoms of emaciation, anorexia, anemia, and decreased productivity [1,3]. Wild mammals, such as puma and feral pigs, can also be infected with *T. evansi* [5,6]. *T. evansi* caused diseases are widely distributed in South America, Asia, Africa, and other regions, causing significant economic losses [7]. Since 2005, several cases of human infection by *T. evansi* have been reported [8–10], suggesting the potential of this parasite to be considered as zoonotic [11]. *T. evansi* parasitizes in the host's blood and is fully exposed to the host's immune surveillance. However, *T. evansi* could evade host-specific immune response by constantly changing variable surface glycoproteins (VSGs) [3]. Suramin is the drug that has most frequently been used for the treatment of surra in horses [12]. There are no vaccines for the prevention of surra. Further understanding of the mechanism of host immune evasion by *T. evansi* will help us to explore new strategies for *T. evansi* control.

Innate immune responses are the first line of defense system developed early in animal evolution [13]. Pathogen-associated molecular patterns (PAMPs) were recognized by Toll-like receptors (TLRs) and activate a series of signaling pathways to produce effector molecules, which ultimately regulate the host immune response [14,15]. TLRs are expressed by immune cells, like macrophages, dendritic cells (DCs), and neutrophils [16]. Macrophages resist parasitic infection through phagocytosis, antigen presentation, and activation of other immune cells [17]. TLRs play a double-edged sword role in parasitic infections. On the one hand, several parasitic protozoa could trigger TLR signaling pathway to protect host from parasite infection. TLR4 could recognize glycoinositolphospholipids (GIPLs) of *T. cruzi* and promote inflammatory response to resist *T. cruzi* infection [18]. TLR2 of human NK cells could be activated by Liposphoglycan of *Leishmania* to release different mediators, such as ROS, inflammatory cytokines, and NO, which in turn help to resist *Leishmania* infection [19]. On the other hand, TLRs could also play a negative role to facilitate parasitic infections. The lipophosphoglycan of *Leishmania* could interact with TLR2 to reduce the expression of TLR9 to inhibit the host immune response [20]. TLR2$^{-/-}$ mice infected with *T. cruzi* could produce more inflammatory cytokines [21]. *Leishmania* RNA virus 1 was recognized by mouse TLR3 to induce the production of inflammatory cytokines, which, however, made mice more susceptible to *Leishmania* infection [22]. Nevertheless, the role of TLRs in *T. evansi* infection was still poorly understood.

EVs are vesicles with membrane structure released by cells [23], which carried a large number of active molecular substances, including protein, lipid, RNA, miRNA, and other regulatory molecules [24]. After pathogen infection, the host could secrete extracellular vesicles containing pathogen components to transmit signals to other cells [25]. At the same time, pathogens such as bacteria [26], fungi [27] and parasites [28–30] could also secrete EVs to regulate the host's immune response. The reticulocyte-derived exosomes infected with *Plasmodium yoelii* carry *P. yoelii* antigen and participate in immune regulation to protect mice from lethal infections [31]. EVs secreted by *Leishmania* contain a variety of virulence factors and non-coding RNAs. These virulence factors play a vital role in promoting the growth of *Leishmania* [24]. *Trichomonas vaginalis* with high adhesion could increase the adhesion of low adhesion parasites to host epithelial cells by transferring exosomes to low adhesion parasites. *T. vaginalis* exosomes could down regulate IL-8 production in Ect cells, which is conducive to the establishment of chronic infection by *T. vaginalis* [32]. *Neospora caninum* EVs could activate the TLR2/MAPK signaling pathway of mouse macrophages to regulate the production of inflammatory cytokines [33]. However, whether *T. evansi* could release EVs to regulate host immune responses in *T. evansi* infection has not been reported.

To investigate the roles of TLRs and TeEVs in *T. evansi* infection, TLR activation and downstream signal pathways induced by *T. evansi* were determined. TeEVs were isolated and characterized. TeKMP-11 was screened by proteomic analysis from TeEVs. *In vitro*, the activation of TLR2-ERK /AKT pathways and the cytokines secretion induced by *T. evansi*, TeEVs, and rTeKMP-11 were examined. In *T. evansi* infected WT, TLR2$^{-/-}$, TLR3$^{-/-}$, TLR4$^{-/-}$ and AKT-blocked mice, the infection rate, survival time, parasite load, cytokines secretion, and

pathological changes were analyzed. Furthermore, the functions of EVs and rTeKMP-11 in *T. evansi* infection were examined *in vivo*. Our results revealed that *T. evansi* evaded the host immune system by releasing EVs to activate TLR2-AKT signaling pathways.

Materials and methods

Animals

TLR2$^{-/-}$, TLR4$^{-/-}$, and TLR3$^{-/-}$ mice were purchased from the Model Animal Research Center of Nanjing University. WT C57BL/6 J mice were purchased from Changsheng Experimental Animal Center in China.

Parasites and cells

Trypanosoma evansi were kept frozen in our laboratory. Mice were infected with 2×10^6 *T. evansi* by intraperitoneal injection. When the number of *T. evansi* in the 1 ml peripheral blood reached 10^8, anticoagulated blood was collected and added an equal volume of phosphate buffered solution containing 1% glucose (PBSG) and centrifuged at 1,000 g for 5 min. The parasites were distributed at the junction of plasma and blood cells. Finally, *T. evansi* was purified by DE52 resin (Solarbio, China) [34]. Briefly, the collected liquid sample containing blood cells and *T. evansi* was loaded onto a column containing DE52 resin and eluted with PBSG. The effluent was collected and centrifuged at 1,000 g for 5 min, then the cell pellet was resuspended with 2 mL RPIM-1640 and counted via a hemocytometer.

Bone marrow-derived macrophages (BMDMs) were isolated as antecedently described [35]. Euthanized mice were immersed in 75% alcohol, the marrow was washed out with RPMI-1640 from the femurs and tibiae. Subsequently, the cells were centrifuged at 300 g for 5 min. Finally, the cells were cultured in RPMI-1640 containing 25% L929-cell conditioned medium, 10% FBS, 1% penicillin and streptomycin (P/S) at 37°C for 7 days. On the seventh day, the cells were resuspended with 200 μL APC anti-mouse/human CD11b (Biolegend, UK) diluted with 1% BSA (1:80) for 2 h, then washed three times and resuspended in 200-μL PBS. The cells were analyzed by flow cytometry.

EVs isolation from *T. evansi*

EVs were purified with a modified protocol [36]. Briefly, the purified *T. evansi* (10^7 cells/mL) was cultured in RPMI-1640 without FBS or P/S for 6 h, then the whole culture was centrifuged at 2,000 g for 10 min to remove parasites and debris. The obtained supernatants were centrifuged at 10,000 g for 45 min and filtration using filter membrane (0.22 μm), then ultracentrifugation at 100,000 g for 70 min. The collected EVs were washed with ice-cold PBS and resuspended in 200 μL PBS. The collected EVs were added to equal volume of RIPA lysate and placed on ice for 40 min. The BCA assay kit (Thermo Scientific, USA) was used to detect the EVs protein concentration. The particle size of TeEVs was ensured by nanoparticle tracking analysis (NTA) with ZetaView PMX 110 (Particle Metrix, Germany).

Scanning and transmission electron microscopy observation for TeEVs

TeEVs were applied onto a copper grid with carbon and 3% phosphotungsticacid to negatively stain the grid. The grid was observed using TEM (HITACHI, Japan).

2×10^7 *T. evansi* were centrifuged at 1,000 g for 5 min and the precipitate was fixed overnight (0.1 M sodium cacodylate buffer contain 2.5% glutaraldehyde). The samples were then fixed with 1% OsO4, dehydrated with ethanol, and embedded in epoxy resin block. Ultrathin section was cut from the block and observed by TEM.

2×10^5 *T. evansi* were plated into 24-well plates loaded with poly-l-lysine-treated (1 mg/mL, Sigma-Aldrich, Germany) coverslips. The cells were fixed with 4% glutaraldehyde for 24 h then washed and fixed in 1.0% osmium tetroxide. Next, the fixed sample was dehydrated in gradient ethanol solutions, then placed in tertiary butyl alcohol, frozen at −20°C, and finally sputtered with gold. The samples were visualized by SEM (Hitachi S-3400 N, Japan).

DiO-labeled TeEVs

TeEVs were labeled and purified with DiO-Membrane EVs Labeling & Purification Kit (Rengen Biosciences, China) according to the manufacturer's instructions. BMDMs were cultured with RPMI-1640 containing 10% FBS and 1% P/S in 24-well plates with glass coverslips and stimulated with the labeled EVs at 37°C. After 2 h treatment, the cells were washed thrice and fixed in 4% paraformaldehyde for 10 min. The cell nucleus was counterstained with DAPI stain, and samples were analyzed with a Laser Scanning Confocal microscope (Olympus FV1000, Japan).

Proteomic analysis of TeEVs

LC-MS/MS was used to analyze the protein composition of TeEVs (Shanghai Omicsspace Biotech Co., Ltd, Shanghai, China). The built-in software Mascot's Proteome Discoverer 2.1 (Thermo Scientific, USA) was used for library search identification and quantitative analysis. The EVs proteome was analyzed using TriTryp DB and Uniprot. HSP 70, EF-1α, Aldolase, and KMP-11 were selected from EVs proteome to be expressed and purified, and the recombinant proteins were used as antigens for polyclonal antibody preparation. Proteomic results were verified by Western blot with aforementioned antibodies.

Cloning, expression, and purification of rTeKMP-11

RNA of *T. evansi* was extracted using the Trizol reagent (Thermo Fisher Scientific, USA). KMP-11 sequence of *T. evansi* was obtained from the TriTrypDB (http://tritrypdb.org/tritrypdb/app, TevSTIB805.9.9950) and amplified by PCR using the primers: KMP-11-F (5′-CGCGGATCCGCGATGGCCACCACATACGAAGA-3′) and KMP-11-R (5′-CCCAAGCTTGGGTCATTTTCCGGGGAACTGGGC-3′). The amplified KMP-11 was ligated into pET-32a vector and expressed in *E. coli* Rosetta DE3 strain (TIANGEN, Beijing, China). The His-Tagged Protein Purification Kit (CWBIO, China) was used to purify the rTeKMP-11 protein. The tag was cut with recombinant bovine enterokinase (Sangon Biotech, Shanghai, China) and removed with the His-Tagged Protein Purification Kit. The protein was dialyzed against PBS at 4°C for at least 5 h, and the buffer solution was changed twice. Endotoxin was removed using Triton X-114 [37]. The endotoxin level was screened by LAL analysis (GenScript, Piscataway, NJ, United States).

Immunofluorescence

2×10^5 *T. evansi* were plated into 24-well cell culture plates loaded with poly-l-lysine-treated coverslips. BMDMs were stimulated with EVs and plated into 24-well cell culture plates. The samples were fixed in 4% glutaraldehyde, and permeabilized using 0.25% Triton X-100. Then, the samples were blocked in 3% BSA and incubated with the anti-KMP-11 antibody (1:100) overnight at 4°C, washed three times and incubated with goat anti-mouse Ig-G conjugated with FITC (Proteintech, Wuhan, China) for 1 h. Nuclear were stained with DAPI. The samples were visualized by a Laser Scanning Confocal microscope.

Mice infection

TLR2$^{-/-}$, TLR3$^{-/-}$, TLR4$^{-/-}$, AKT-blocked WT and WT mice (n = 10 per group) were infected with 1×10^4 *T. evansi* by intraperitoneal injection. MK-2206 (120 mg/kg, every 2 days by p.o., Selleck, USA) was used to block the AKT pathway *in vivo* [38]. Blood samples were collected from tail vein every day to detect the parasite load, and the serum was collected for cytokines detection. The time of death was recorded. The spleen and lung of mice were harvested on the fifth day post infection (dpi) for HE-staining.

To explore the role of EVs in *T. evansi* infection, mice (n = 10 per group) were infected with 1×10^4 *T. evansi* by intraperitoneal injection. Meanwhile, 50 µg/mL EVs were injected intravenously (tail vein) into the mice for three consecutive days. In control group, an equal volume of sterile PBS was injected in mice.

To understand the role of rTeKMP-11 protein in the pathogenesis of *T. evansi*, mice (n = 10 mice per group) were pretreated with 50 µg/mL rTeKMP-11 protein or the empty carrier protein (ECP) coated with 100 µg DOTAP liposome (final volume 120 µL) using DOTAP Liposomal Transfer Reagent (Roche, Indianapolis, IN) by intravenously injection into tail vein for three consecutive days. DOTAP was used as the negative control. Meanwhile, mice were infected with 1×10^4 *T. evansi* by intraperitoneal injection. Blood samples from all mice treated with EVs, rTeKMP-11 protein, ECP, and DOTAP control were collected from tail vein every day to detect the parasites load, and the serum was collected for cytokines detection. The mice were monitored after infection, and the times of death time for the mice were recorded.

Real-time quantitative PCR analysis

3×10^6 WT mouse BMDMs were stimulated with 3×10^6 *T. evansi* or 50 µg/mL TeEVs for 4 h, respectively. The RNA of cells was extracted and reverse-transcribed to cDNA. RT-qPCR was performed at 95°C for 10 min, followed by 40 cycles of 95°C for 30 s, 58°C for 30 s and 72°C for 30 s, with a final extension step at 72°C for 10 min. The data were normalized to GAPDH. Primers were designed using the NCBI Primer-BLAST tool (https://www.ncbi.nlm.nih.gov/tools/primer-blast/) and synthesized by Kumei Biotechnology Co., Ltd (Changchun, China). The primers are listed in Table 1.

Table 1. Primers used for Real-time PCR.

Gene	Sequence 5′-3′
TLR 1F	CGAAAAAGAAGACCCCGAATC
TLR 1R	GACGGACAGATCCAGAACAAAAG
TLR 2F	CGCTCCAGGTCTTTCACCTC
TLR 2R	AGGTCACCATGGCCAATGTA[33]
TLR 3F	AAGACAGAGACTGGGTCTGGG
TLR 3R	AAGGACGCCTGCTTCAAAGT
TLR 4 F	ACTGTTCTTCTCCTGCCTGACA
TLR 4 R	GGACTTTGCTGAGTTTCTGATCC
TLR 5 F	TTGGACTTGGGCCAAAGC
TLR 5 R	CTGGAGAGTCCACAGGAAAACA
TLR 6 F	TCCGACAACTGGATCTGCTC
TLR 6 R	AAGACTTTCTGTTTCCCCGC
TLR 7 F	ATACAGCTCAGCAAAAAGACAGTGT
TLR 7 R	TCCAGGAGCCTCTGATGAGA
TLR 8 F	CTGACGTGCTTTTGTCTGCTG
TLR 8 R	AGGGAGTTGTGCCTTATCTCGT
TLR 9 F	CTAGATGCTAACAGCCTCGCC
TLR 9 R	GTCACCTTCACCGCTCCTG
TLR 11 F	GGGACTTTGGGATTGGAAAT
TLR 11 R	CTAAGGCCTGTCCTGTGAGC
TLR 12 F	CCTTGAGGGTATGGGGTGC
TLR 12 R	GGGGCTGGGTTATGGACTG
TLR 13 F	AAAGACACGGGATTCAGGTTG
TLR 13 R	GGTGGTCCAGGAATACAGAGG
GAPDH F	CCATGTTTGTGATGGGTGTG
GAPDH R	CCTTCTTGATGTCATCATAC[33]

Western blot analysis

3×10^6 WT mouse BMDMs were stimulated with 3×10^6 *T. evansi*, 50 μg/mL EVs, or 50 μg/mL rTeKMP-11 protein, and the cells at different time points were collected (0, 2, 4, 6, and 8 h). The protein samples of BMDMs cells, *T. evansi* and EVs were prepared with radioimmunoprecipitation assay (RIPA) lysis buffer (Beyotime, Shanghai, China) with 1 mM phenylmethanesulfonyl fluoride (PMSF, Sigma-Aldrich, USA). The proteins (30 μg) was separated by SDS-PAGE (12%) electrophoresis and transferred to PVDF membranes (Millipore, Bedford, MA, USA). Membranes were blocked with 5% skim milk for 2 h and incubated overnight at 4°C with the following antibodies: rabbit anti-p-P38, anti-total P38, anti-p-P65, anti-total P65, anti-p-ERK1/2, anti-total ERK1/2, anti-p-AKT, anti-total AKT, anti-GAPDH (Cell Signaling Technology, USA) mouse anti-HSP70, anti-Aldolase, anti-EF-1α, and anti-KMP-11 (mouse polyclonal antibodies). After washing 3 times with TBS-0.05% Tween 20 for 15 min, the blots were incubated with secondary HRP-conjugated antibodies (Proteintech, Wuhan, China) for 1 h and washed as before. Finally, target proteins were visualized using ECL luminous reagent (Millipore, Bedford, MA, USA). Protein expressions were quantified using Image J 2.0 software.

Cytokines detection by ELISA

WT/TLR2$^{-/-}$ mouse BMDMs (3×10^6) were seeded into 6-well plates and incubated with 3×10^6 *T. evansi*, 50 μg/mL EVs or 50 μg/mL rTeKMP-11 protein. For the kinase inhibition test, BMDMs were pretreated with inhibitors of P38 (SB203580, 30 μM, Sigma-Aldrich), ERK (PD98059, 40 μM, Sigma-Aldrich), or AKT (AKT inhibitor IV, 5 μM, Santa Cruz; MK-2206, 1 μM, Selleck), respectively, and then stimulated with *T. evansi*, EVs, or rTeKMP-11 protein. The culture supernatants were harvested for ELISA assay at 8, 12, 18, and 24 h post stimulation.

The blood of infected or uninfected *T. evansi* mice was collected and the serum was collected for ELISA measurement. IL-1β, IL-2, IL-4, IL-6, IL-12p40, TNF-α, IL-17A, and IFN-γ were measured by Cytokine ELISA Ready-SET-Go kits (Thermo Scientific, USA) according to the instructions.

Determination of *T. evansi* viability

3×10^6 *T. evansi* were incubated with different concentrations of MK-2206 (2 nM, 50 nM, 500 nM and 1 μM) for 12 h to detect the effect of MK-2206 on *T. evansi* viability. 3×10^6 BMDMs were pretreated with MK-2206 (1 μM) for 60 min, then removed the supernatants and incubated with 3×10^6 *T. evansi* for 12 h to detect the effect of MK-2206 treated BMDMs on *T. evansi* viability. 3×10^6 *T. evansi* were co-cultured with IL-12p40 (100 pg/mL, Abcom, USA) treated BMDMs to detect the effect of IL-12p40 treated BMDMs on *T. evansi* viability. All cell supernatants were collected and stained with 10% trypan blue (Sigma-Aldrich, USA) for 2 min. The dead *T. evansi* were stained blue, while the living *T. evansi* were unstained. Subsequently, all alive *T. evansi* were counted via a hemocytometer.

Statistical analysis

The data were analyzed by One-Way ANOVA using SPSS version 19.0 (SPSS, Inc., Chicago, IL, USA) and were expressed by mean ± standard error of the mean (SEM) of triplicate experiments. All charts were generated by GraphPad prism 7.00 (GraphPad InStat Software, San Diego, CA). The asterisk indicated the statistically significant difference: *, $P < 0.05$; **, $P < 0.01$; ***, $P < 0.001$; ns, not significant.

Results

TLR2$^{-/-}$ mice were more resistant to *T. evansi* infection compared with WT mice.

The isolated BMDMs were identified by flow cytometry and the purity was 96.62% (Figure S1). 3×10^6 WT mouse BMDMs were stimulated with *T. evansi*. After
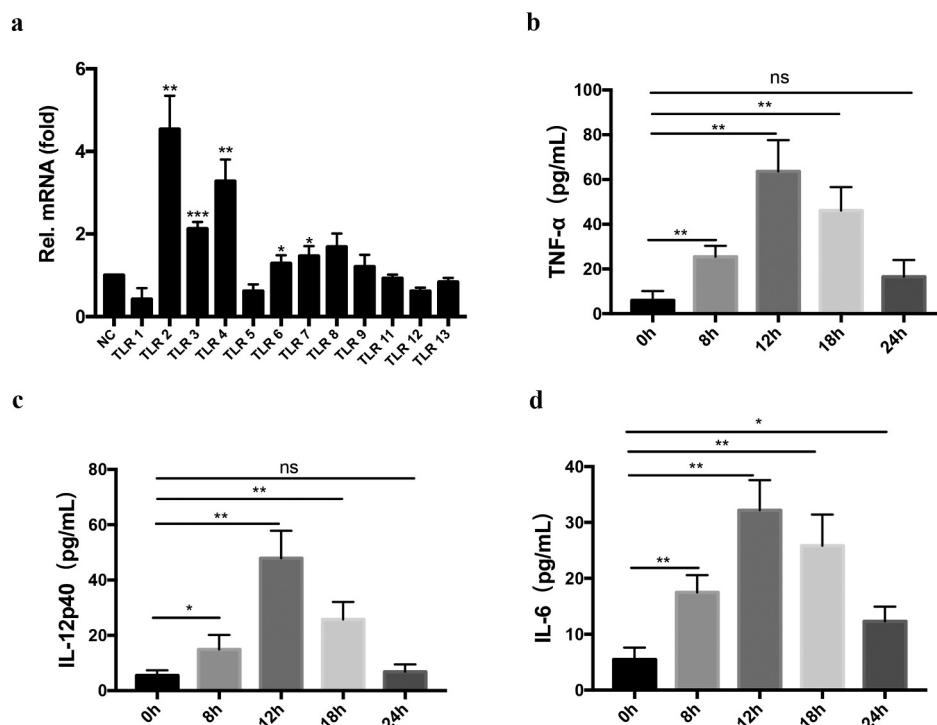
Figure 1. *T. evansi* activated TLRs and induced inflammatory cytokines secretion in BMDMs. (a) 3×10^6 WT mouse BMDMs incubated with 3×10^6 *T. evansi* or medium alone, respectively. The relative mRNA levels of TLRs in total RNAs were analyzed by RT-qPCR. (b-d) WT mouse BMDMs were incubated with *T. evansi*, cytokines secretion in the supernatants were detected using ELISA assay. The data are presented as the mean ± SEM from at least three independent experiments. ns, not significant; *, $P < 0.05$; **, $P < 0.01$; ***, $P < 0.001$ VS the negative control group.

co-incubation for 4 h, compared with control, the transcriptional levels of TLR2, TLR3, and TLR4 were significantly up-regulated (Figure 1a).

A pilot experiment had determined that 1×10^4 *T. evansi* could result in 100% parasitemia in WT mice via intraperitoneal injection (Figure S2A), which was set as the baseline to describe the parasitemia in TLR2$^{-/-}$, TLR3$^{-/-}$, and TLR4$^{-/-}$ mice. For parasite infection, 1×10^4 *T. evansi* was intraperitoneally injected into WT, TLR2$^{-/-}$, TLR3$^{-/-}$, and TLR4$^{-/-}$ mice, respectively. Results indicated that TLR2$^{-/-}$ mice showed higher resistance to *T. evansi* infection compared with WT, TLR3$^{-/-}$, and TLR4$^{-/-}$ mice. The parasitemia in WT, TLR3$^{-/-}$, and TLR4$^{-/-}$ mice were 100%, while the parasitemia in TLR2$^{-/-}$ mice was 83.3% (Figure 2a). The longest survival times of WT, TLR2$^{-/-}$, TLR3$^{-/-}$, and TLR4$^{-/-}$ mice infected with *T. evansi* were 6, 9, 6, and 6 days, respectively (Figure 2b). The parasitemia of WT, TLR3$^{-/-}$, and TLR4$^{-/-}$ -infected mice reached the peak on the sixth day and died (3×10^8/mL), while the parasites load of TLR2$^{-/-}$infected group was significantly lower than that of WT-infected group, and the number of parasites in the TLR2$^{-/-}$infected group

decreased significantly on the seventh day, increased again on the eighth day, and reached the peak of parasitemia on the ninth day (Figure 2c, S2B).

WT and TLR2$^{-/-}$ mice were euthanized at 5 dpi, and the pathological sections of the spleen and lung were analyzed. In WT-infected group, the spleens were hyperemic and a large amount of iron swallowing cells were observed. Interstitial widening and inflammatory exudate in the alveoli were observed. The TLR2$^{-/-}$infected mice had significantly milder pathological changes than that in the WT-infected mice (Figure 2d). These results indicated that TLR2$^{-/-}$ mice were more resistant to *T. evansi* infection.

IL-12 [39], IFN-γ [40], and TNF-α [41] play vital roles against *Trypanosoma* infection. The cytokine levels (IL-1β, IL-2, IL-4, IL-6, IL-12p40, IL-17A, TNF-α, and IFN-γ) in the serum at different times (0, 1, 2, 3, 4, and 5 dpi) were measured. The IFN-γ and IL-12p40 levels in TLR2$^{-/-}$infected mice were significantly higher than that of the WT-infected mice up to 4 dpi. However, the IFN-γ and IL-12p40 secretions in the WT-infected mice was significantly higher than that of the TLR2$^{-/-}$infected
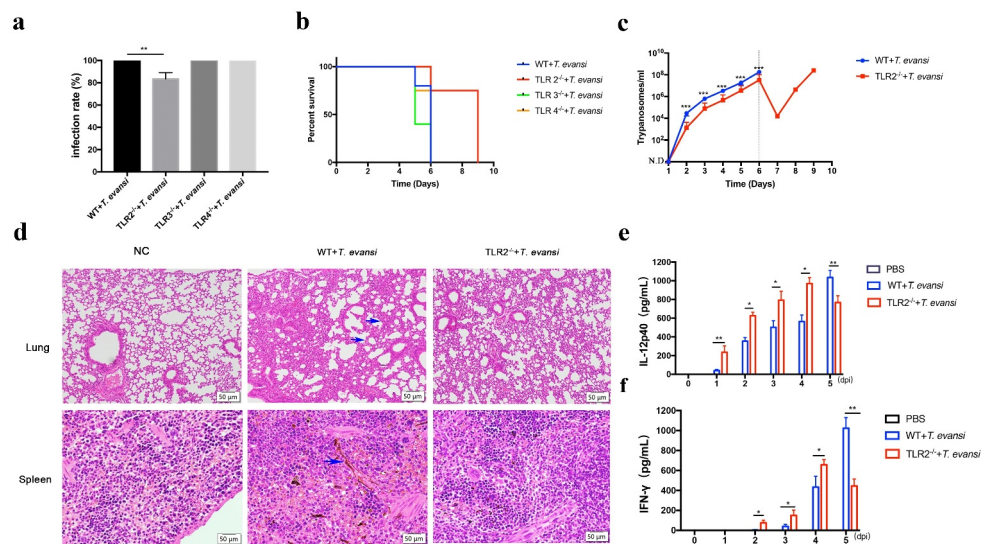
Figure 2. The TLR2$^{-/-}$ mice were more resistant to _T. evansi_ infection than the WT mice. (a) WT, TLR2$^{-/-}$, TLR3$^{-/-}$, and TLR4$^{-/-}$ mice were infected with 1×10^4 _T. evansi_ by intraperitoneal injection, respectively (n = 10 mice per group). The infection rate of mice was detected. (b) The death times of WT, TLR2$^{-/-}$, TLR3$^{-/-}$, and TLR4$^{-/-}$ mice-infected were recorded. (c) Parasite load was measured in peripheral blood of WT and TLR2$^{-/-}$ mice. (d) Hematoxylin-and-eosin staining of lung and spleen sections. (e, f) ELISA analysis of IL-12p40 and IFN-γ levels in the serum of WT and TLR2$^{-/-}$ mice infected with _T. evansi_. The values are shown as the mean ± SEM from three independent experiments. *, $P < 0.05$; **, $P < 0.01$ for the WT group versus the TLR2$^{-/-}$ group.

mice at 5 dpi (Figure 2 e, f). _T. evansi_ infection induced the production of IL-6 in both WT and TLR2$^{-/-}$ mice, no significant difference was observed between the two infected groups (Figure S3). There was no significant difference in the secretion of IL-1β, IL-2, IL-4, IL-17 and TNF-α in all infected mice.

T. evansi induced low-level secretion of cytokines via TLR2-mediated ERK pathway in BMDMs.

Cytokines secretion (IL-1β, IL-2, IL-4, IL-6, IL-12p40, IL-17A, INF-γ, and TNF-α) induced by _T. evansi_ in the culture supernatant of BMDMs at different time points (8, 12, 18, and 24 h) were detected. The results showed that _T. evansi_ could induce low-level secretion of TNF-α IL-6, and IL-12p40. TNF-α (63.67 ± 8.066 pg/mL), IL-12p40 (47.92 ± 5.717 pg/mL), and IL-6 (37.17 ± 3.118 pg/mL) secretions reached the maximum at 12 h (Figure 1b, c, d). Secretion of other five cytokines could not be detected in _T. evansi_ stimulated mouse BMDMs. IL-6, IL-12p40, and TNF-α in BMDMs of WT or TLR2$^{-/-}$ mice stimulated with _T. evansi_ were detected at 12 h. The results showed that IL-12p40 in the TLR2$^{-/-}$ group (186.4 ± 8.573 pg/mL) was significantly higher ($P < 0.001$) than that in the WT group (46.96 ± 6.286 pg/mL), while TNF-α and IL-6 were not significantly different (Figure 3a).

Subsequently, we examined several common inflammatory pathways, like NF-κB and MAPK. _T. evansi_

could significantly activate TLR2 ($P < 0.001$) and ERK ($P < 0.001$) pathways after stimulation for 4 h and 6 h, respectively (Figure 3 b, c). But no obvious changes were observed for p-P38 and p-P65 (Figure S4). In order to study whether TLR2 played a regulatory role, we used _T. evansi_ to stimulate BMDMs of WT or TLR2$^{-/-}$ mouse and the results suggested that the phosphorylation level of ERK ($P < 0.001$) was significantly inhibited in TLR2$^{-/-}$ group (Figure 3e, f).

BMDMs were pre-treated with ERK inhibitors and stimulated with _T. evansi_. The results showed that _T. evansi_-induced the secretion of IL-6 ($P < 0.01$), IL-12p40 ($P < 0.01$), and TNF-α ($P < 0.01$) were significantly decreased in ERK-blocked BMDMs (Figure 3d).

T. evansi caused serious Trypanosomiasis by inhibiting the secretion of inflammatory cytokines via TLR2-mediated AKT pathway

Trypanosoma evansi could induce AKT activation after stimulation for 2 h and maintained at a high level (Figure 4a, b). To explore the role of the AKT pathway in regulating cytokines secretion, BMDMs were pre-treated with AKT inhibitor IV. In AKT inhibitor group, the production of IL-12p40 (117.8 ± 12.2 pg/mL), IL-6 (64.31 ± 9.138 pg/mL), and TNF-α (132.9 ± 19.01 pg/mL) induced by _T. evansi_ were significantly increased (Figure 4c).
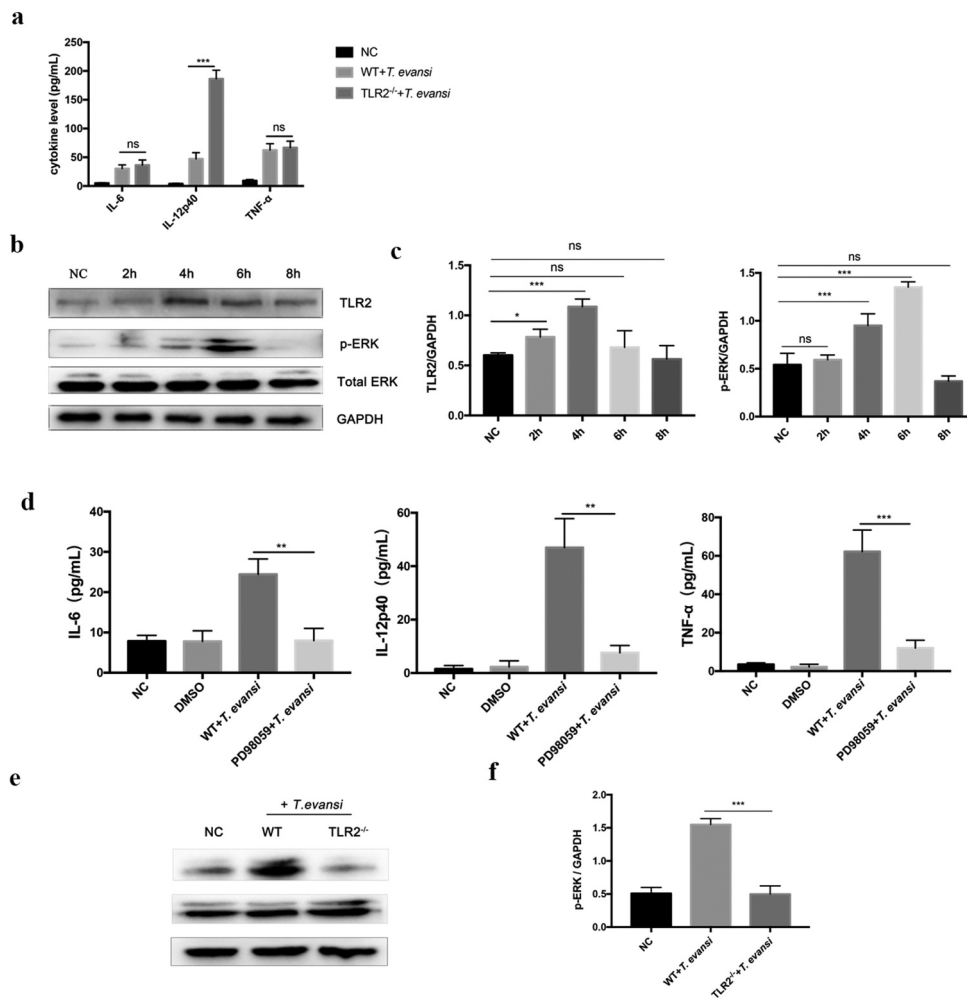
Figure 3. *T. evansi* promoted inflammatory cytokines secretion via TLR2-mediated ERK pathway. (a) WT/TLR2$^{-/-}$ mouse BMDMs were stimulated with *T. evansi* for 12 h. The cytokines secretion levels were analyzed by ELISA. (b, c) WT BMDMs were stimulated with *T. evansi*, the levels of phosphorylation of ERK were analyzed by Western blot. (d) WT mouse BMDMs were stimulated with *T. evansi* after pretreated with inhibitor of ERK (PD98059; 40 μM) for 60 min. The amount of cytokines secretion was detected by ELISA. (e, f) WT/TLR2$^{-/-}$ BMDMs were stimulated with *T. evansi* for 6 h, then the p-ERK expression was determined by immunoblot and densitometric analysis. Bars represent the mean ± SEM from three independent experiments. *, $P < 0.05$; **, $P < 0.01$; ***, $P < 0.001$; ns, not significant, for the WT group versus the TLR2$^{-/-}$ group, or negative control group versus experimental group, or ERK inhibitor stimulation group versus WT stimulation group.

BMDMs from TLR2$^{-/-}$ and WT mice were stimulated with *T. evansi* for 6 h, the phosphorylation level of AKT ($P < 0.05$) was significantly inhibited in BMDMs from TLR2$^{-/-}$ mice compared to that from WT mice (Figure 4d, e).

MK-2206 is another AKT inhibitor that often used *in vivo* assay. The effect of MK-2206 on *T. evansi in vitro* was performed. The result showed that MK-2206 did not affect parasite viability at concentrations of 0.02 μM to 1 μM *in vitro* (Figure S5A). Then *T. evansi* were co-incubated with WT mouse BMDMs pretreated with MK-2206 (1 μM) for

60 min. After 12 h co-incubation, parasites viability and the secretions of IL-12p40, IL-6 and TNF-α were examined. The results showed that the *T. evansi* viability was 27.23% in MK-2206-untreated group compared with 14.03% in the MK-2206-treated group (Figure S5B). In MK-2206-treated group, the production of IL-12p40 (104.9 ± 6.209 pg/mL), IL-6 (62.84 ± 5.485 pg/mL), and TNF-α (116.5 ± 7.517 pg/mL) induced by *T. evansi* were significantly increased (Figure S5C). We detected the effect of IL-12p40 on *T. evansi in vitro*. *T. evansi* were co-incubated with WT mouse BMDMs treated with
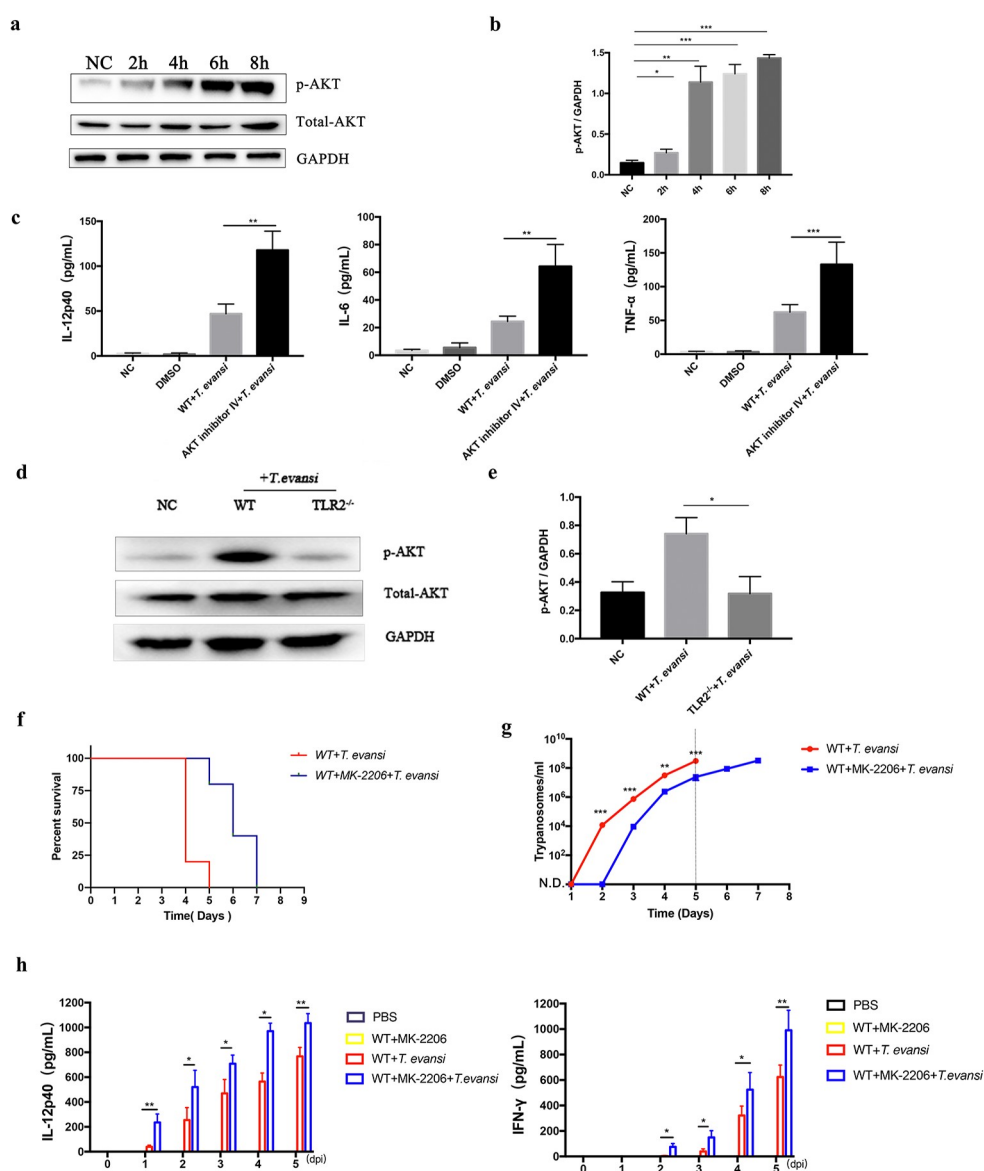
Figure 4. ***T. evansi* inhibited the secretion of inflammatory cytokines via TLR2-mediated AKT pathway**. (a, b) WT mouse BMDMs were stimulated with *T. evansi*, Western blot and densitometric analysis were used to detect the phosphorylation level of AKT. (c) WT mouse BMDMs stimulated with *T. evansi* after pretreated with AKT inhibitor IV for 60 min. ELISA analysis of TNF-α, IL-6, and IL-12p40 levels. (d, e) WT/TLR2$^{-/-}$ mouse BMDMs were stimulated with *T. evansi* for 4 h, and then the p-AKT expression was determined by immunoblot and densitometric analysis. (f) WT mice (n = 10 mice per group) were administered with MK-2206 to block AKT or without, then infected with 1×10^4 *T. evansi* by intraperitoneal injection. The death time was recorded. (g) The parasites load in peripheral blood was detected. (h) ELISA analysis of IL-12p40 and IFN-γ levels in the serum of AKT-blocked and WT mice infected with *T. evansi*. Bars represent the mean ± SEM for three independent experiments. *, $P < 0.05$; **, $P < 0.01$; ***, $P < 0.001$, for negative control group versus experimental group, or AKT inhibitor group versus without AKT inhibitor group, or the WT group versus the TLR2$^{-/-}$ group.

IL-12p40 (100 pg/mL) for 12 h. The results showed that the *T. evansi* viability was 30.43% in IL-12p40-untreated group compared with 16.83% in the IL-12p40-treated group (Figure S5D).

To explore the role of AKT in *T. evansi*-infected mice, WT and AKT-blocked (MK-2206 treatment) mice were infected with *T. evansi*. WT-infected mice

began to die on the fourth day and all died on the fifth day after infection, while the AKT-blocked mice began to die on the fifth day and all died on the seventh day after infection (figure 4f). The parasites could be detected in the peripheral blood of WT mice on the second day after infection and reached the parasitemia on the fifth day (3×10^8/

mL), while the parasites could be detected in the AKT-blocked mice on the third day and the number of parasites was significantly lower than WT mice (Figure 4g). IL-12p40 and IFN-γ secretions in the serum of AKT-blocked mice infected with *T. evansi* were significantly higher than that of WT mice (Figure 4h).

T. evansi could continuously secrete EVs.

Negative staining observations using TEM showed that TeEVs were partially flat ball-shaped, with a double-layer membrane structure, and about 70–150 nm in diameter (Figure 5a). NTA showed that the mean diameter of the EVs was 110 nm (Figure S6). SEM results showed that the posterior end of *T. evansi* could extend out the nanotubes about 100 nm in diameter and TeEVs could be found on the surface of the parasite (Figure 5b). Ultrathin section observations revealed that free EVs and the nanotubes had similar membrane structures with the cell plasma membrane, and the nanotubes could dissociate to produce free EVs (Figure 5c).

TeEVs regulated inflammatory cytokines secretion via TLR2-mediated AKT/ERK pathways in BMDMs

Labeled EVs were co-incubated with BMDMs for 2 h and EVs were observed to be internalized into BMDMs (Figure 6a). WT mouse BMDMs were stimulated with TeEVs for 4 h. RT-qPCR results showed that EVs could significantly activate TLR2, TLR3, and TLR4 in BMDMs (Figure 6b). The low-level secretion of IL-12p40, IL-6, and TNF-α in the culture supernatants of BMDMs stimulated with EVs were detected (Figure 6c-e). The EVs-induced IL-12p40 secretion ($P < 0.001$) in TLR2$^{-/-}$ BMDMs was significantly higher than that in WT BMDMs. However, no significant differences were detected in IL-6 and TNF-α secretions (figure 7f).

EVs could activate ERK and AKT pathways (Figure 7a, b), and the phosphorylation levels of ERK and AKT were significantly decreased in TLR2$^{-/-}$ mice BMDMs (Figure 7c, d). The secretion levels of IL-12p40, IL-6, and TNF-α decreased significantly after ERK inhibitor pretreatment, while the secretion levels of IL-12p40 ($P < 0.01$), IL-6 ($P < 0.01$), and TNF-α ($P < 0.01$) was increased significantly after AKT inhibitor pretreatment (Figure 7e). These results suggested that TeEVs played an important role in TLR2-mediated ERK and AKT activation, which ultimately regulated the secretion of inflammatory cytokines.

TeEVs promoted *T. evansi* proliferation and accelerated mice's death *in vivo*

Trypanosoma evansi-infected mice in the EV group began to die on the fourth day, and all died on the fifth day, while *T. evansi*-infected mice in the PBS group began to die on the fifth day, and all died on the seventh day (Figure 8a). The parasite load of *T. evansi*-infected mice with EVs treatment was higher than that of PBS treated mice (Figure 8b). IL-12p40 and IFN-γ secretions in the EVs treated mice were significantly lower than that in the PBS treated mice (Figure 8c).

Proteomic analysis of TeEVs

Proteomics results showed that 746 proteins were identified in TeEVs, of which at least two unique peptides accounted for 57.5% (429/746). The proteins identified in TeEVs were similar to those reported in *T. brucei* [36] (Table 2). The ribosomal proteins in the TeEVs proteome were detected. HSP-70, EF-1α, KMP-11, and Aldolase were confirmed by Western blot (Figure 9a). The proportion of biological process [42], cell component (CC) and molecular function (MF) of the proteins were shown in Figure 9b. Among all of the identified proteins, 595 proteins were involved in 78 signal pathways, the top five of which were Proteasome, Aminoacyl-tRNA biosynthesis, RNA transport, Ribosome, and mRNA surveillance pathway (Figure 9c). In addition, these proteins were also related to PI3K-AKT, MAPK, NOD-like, and toll-like signaling pathways.

T. evansi KMP-11 recombinant protein activated AKT pathway *in vitro* and promoted *T. evansi* proliferation *in vivo*

First, rTeKMP-11 protein was expressed and purified (Figure 10a). TeKMP-11 protein was detected in BMDMs stimulated with TeEVs and rTeKMP-11 for 2 h, indicating that EVs could release their cargo into BMDMs and rTeKMP-11 could enter the cytoplasm of BMDMs (Figure 10b). Then we detected the location of KMP-11 protein in *T. evansi*. The results showed that TeKMP-11 protein mainly existed in parasite coat, the flagellum, and the flagella pocket (Figure 10c). After stimulating BMDMs with different concentrations of rTeKMP-11, we analyzed the cell viability and selected the concentration of 50 μg/mL for subsequent experiments (Figure S7). Cytokines secretion and MAPK, AKT, and NF-κB pathways in BMDMs stimulated with rTeKMP-11 were examined. The secretion levels
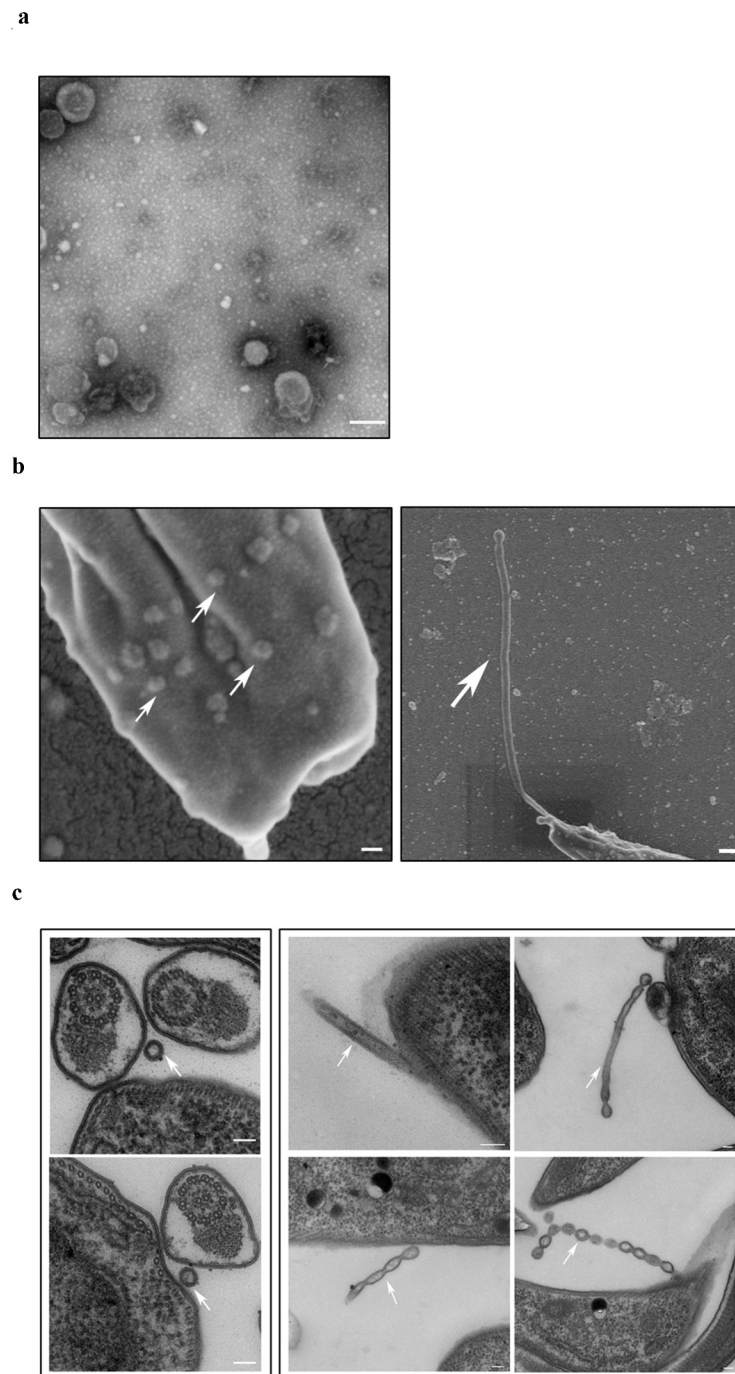
Figure 5. Physical characterizations of TeEVs. (a) The partially flat ball-shaped vesicles were observed using negative staining by TEM. Scale bar = 100 nm. (b) EVs on the surface of *T. evansi* (left, scale bas = 100 nm) and the nanotubes protruded from the posterior end of *T. evansi* (right, scale bar = 200 nm) were visualized by SEM. (c) Thin section TEM analysis of EVs (left) and nanotubes (right). The membranes of EVs and nanotubes were similar to the cell plasma membrane and the nanotubes were dissociated to produce free EVs. Scale bars = 100 nm.

of IL-12p40 (64.24 ± 4.214 pg/mL), IL-6 (65.95 ± 10.99 pg/mL), and TNF-α (112.6 ± 14.69 pg/mL) reached the maximum at 12 h after stimulation of BMDMs by rTeKMP-11 (Figure 10d), and the control carrier protein had no effect on the production of cytokines in BMDMs (Figure 10e). The phosphorylation level of P38 peaked at 2 h and returned to baseline at 6 h and the phosphorylation level of AKT

Figure 6. TeEVs could activate TLR2 and induce cytokines secretion in BMDMs. (a) After incubating the labeled EVs with BMDMs for 2 h, the internalization of EVs by BMDM was observed by confocal laser scanning. Green: labeled EVs. Blue: nuclei. Scale bar = 5 μm. (b) WT mouse BMDMs were incubated with TeEVs or medium alone, respectively. RT-qPCR was used to analyze the relative mRNA level of TLRs in total RNA. (c-e) After WT mouse BMDMs and EVs were co-incubated, the secretion of cytokines was detected by ELISA assays. Bars 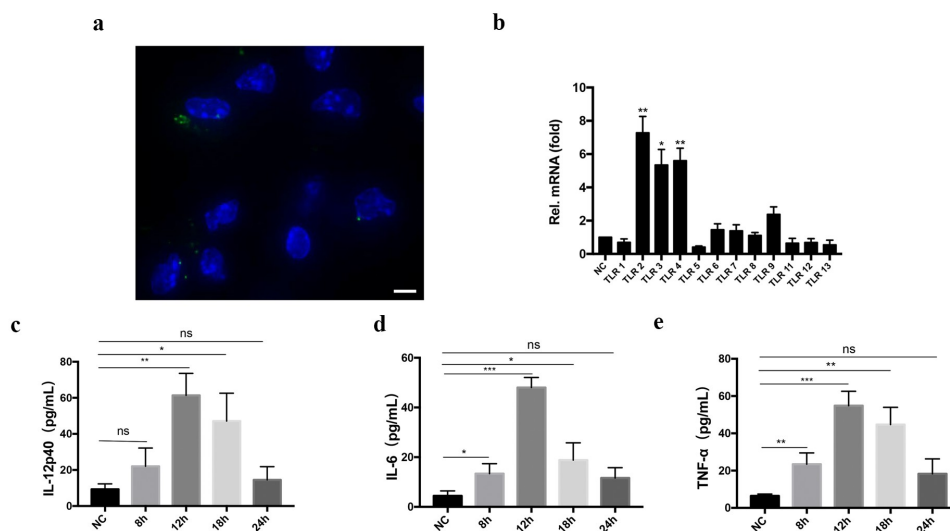represent the mean ± SEM of triplicate experiments. ns, not significant; *, $P < 0.05$; **, $P < 0.01$; ***, $P < 0.001$ VS the negative control group.

maintained at a high level (Figure 10f, g). The production of IL-12p40, IL-6, and TNF-α increased significantly after treatment with AKT inhibitor and reduced significantly using P38 inhibitor (Figure 10h).

To study the role of KMP-11 protein *in vivo*, animal experiments were conducted. The results showed that *T. evansi*-infected mice in the rTeKMP-11 group began to die on the fourth day, and all died on the fifth day, while the mice in the ECP and DOTAP groups began to die on the fifth day, and all died on the seventh day (Figure 10i). The parasite load of *T. evansi*-infected mice injected with rTeKMP-11 was higher than that of ECP and DOTAP groups (Figure 10j). Finally, we tested the cytokines in the serum by ELISA at different times (0, 1, 2, 3, 4, and 5 dpi). IL-12p40 and IFN-γ secretions in the rTeKMP-11 group was significantly lower than that in the ECP and DOTAP groups (Figure 10k).

Discussion

Trypanosomas have developed a successful immune escape mechanism. Antigen variation of variant surface glycoproteins (VSGs) was the most important immune escape mechanism in *Trypanosomes*, which is to avoid the host's humoral response by constantly converting VSGs [43]. *Trypanosomas* could activate the polyclonal B cells to differentiate into short-lived plasmablasts, which ultimately lead to apoptosis/elimination of the B cell population

[41,44–46]. As an important bloodborne protozoa, the immune evasion mechanism of *T. evansi* deserves more investigation. The results from the present study showed that *T. evansi* could secrete TeEVs to activate TLR2-AKT pathway, which in turn inhibited the productions of inflammatory cytokines to allow the survival of parasites. In addition, TeKMP-11 protein, a component of TeEVs, was shown to be involved in promoting *T. evansi* infection.

TLR2 plays a vital role in fighting parasite infections, including *T. congolense, P. yoelii, T. gondii*, and *L. major* [47–50]. However, it also plays a negative role to promote parasite infection. TLR2$^{-/-}$ mice exhibited reduced severity of giardiasis through increased production of inflammatory cytokines [51]. TLR2$^{-/-}$ mice had a lower parasite load than C57BL/6 wild-type mice in the first two weeks after *L. amazonensis* infection [52]. In this study, we found that *T. evansi* could activate TLR2, TLR3 and TLR4 in mouse BMDMs. Compared with TLR3$^{-/-}$, TLR4$^{-/-}$, and WT mice, TLR2$^{-/-}$ mice were more resistant to *T. evansi* infection mainly due to decreased infection rate and the parasites load, delayed survival time and relieved pathological changes.

Proinflammatory cytokines IL-12 and IFN-γ played vital roles in *Trypanosoma* infections [53,54]. The secretion of IL-12-dependent IFN-γ was essential for fighting against *T. brucei brucei* and *T. evansi* infections [55]. Studies have shown
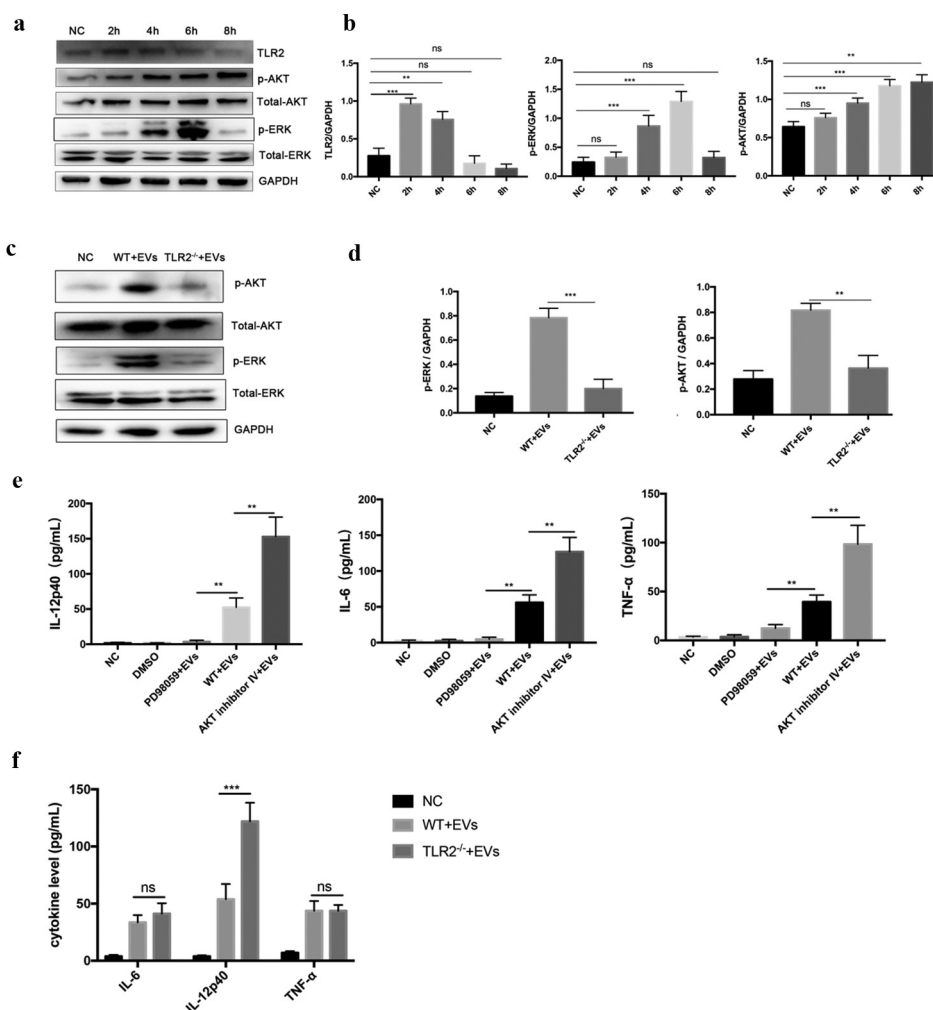
Figure 7. TeEVs regulated inflammatory cytokines secretion via TLR2-mediated AKT/ERK pathways. (a, b) After WT mouse BMDMs and TeEVs were co-incubated, Western blot and densitometric analysis were used to measure the phosphorylation levels of ERK and AKT. (c, d) The BMDMs of WT/TLR2$^{-/-}$ mouse were stimulated with TeEVs for 6 h, the p-ERK and p-AKT expression were determined by immunoblot and densitometric analysis. (e) WT mouse BMDMs were stimulated with EVs after pretreated with PD98059 or AKT inhibitor IV for 60 min. The secretion levels of cytokines were measured by ELISA. (f) BMDMs of WT/TLR2$^{-/-}$ mouse with EVs were co-incubated for 12 h. The cytokine levels were measured by ELISA. Bars represent the mean ± SEM from three independent experiments. ns, no significance; **, $P < 0.01$; ***, $P < 0.001$ for the stimulated group versus the negative control group, or AKT/ERK inhibitor stimulation group versus WT stimulation group, or the WT group versus the TLR2$^{-/-}$ group.

that IL-1, IFN-γ, IL-6, and TNF-α were increased in serum after *T. evansi* infection in rats [56]. In this study, IFN-γ and IL-12p40 secretions were significantly higher in TLR2$^{-/-}$ mice than in WT mice at 2, 3, and 4 dpi, suggesting that IL-12p40 and IFN-γ might be critical in resisting *T. evansi* infection. BALB/c mice that were susceptible to African trypanosomes showed higher level of IL-6 in BMDMs than C57BL/6 J mice with relative resistance [57]. The use of anti-IL-6 monoclonal antibody did not reduce the number of *T. cruzi* in blood or tissues [58]. Our results showed that IL-6 secretion in serum of WT and TLR2$^{-/-}$ mice infected with *T. evansi* was increased, but there was no significant

difference between the two groups. This result indicated that the secretion of IL-6 induced by *T. evansi* might not be regulated by TLR2 and did not play a significant role in resisting trypanosome infection. Interestingly, *T. evansi* could suppress multiple cytokine secretions that might help to maintain parasites survival in blood.

Macrophages play an important role in controlling parasite infections in many protozoa [59,60]. A complete monocyte system was essential to start and maintain the anti-*Trypanosoma* response [61]. Macrophages are the major source of inflammatory cytokines in *T. evansi* infection [62] However, the intracellular signaling pathway by which *T. evansi*
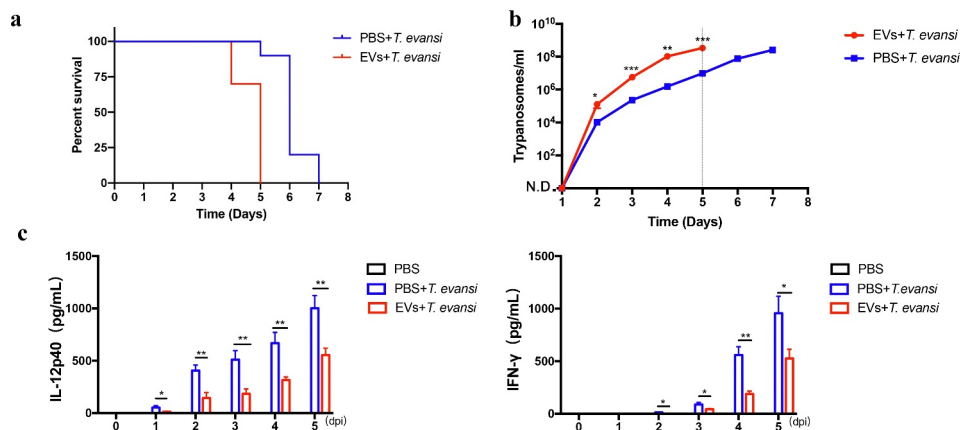
Figure 8. TeEVs could promote *T. evansi* proliferation *in vivo*. WT mice (n = 10 mice per group) were infected with 1×10^4 *T. evansi* by intraperitoneal injection. 50 μg EVs were injected intravenously (tail vein) into the mice for three consecutive days. Control mice were injected with an equal volume of PBS. (a) The death time was recorded daily. (b) Parasites load in peripheral blood was detected daily. (c) The production levels of IL-12p40 and IFN-γ in the serum were detected by ELISA. Bars represent the mean ± SEM of three independent experiments. *, $P < 0.05$; **, $P < 0.01$ for PBS group versus EVs group.

Table 2. Top 50 proteins enriched in extracellular vesicles of *T. evansi*.

Proteins	Peptides	PSMs	Unique Peptides	gene ID
alpha tubulin	15	81	15	TevSTIB805.1.2250
Tubulin beta chain	17	78	12	TevSTIB805.1.2240
enolase	16	46	16	TevSTIB805.10.3130
nucleolar protein, putative	12	44	13	TevSTIB805.8.3860
elongation factor 1-alpha, EF-1-alpha	12	41	11	TevSTIB805.10.2260
glyceraldehyde 3-phosphate dehydrogenase, glycosomal	16	37	10	TevSTIB805.6.4410
40S ribosomal protein S2, putative	11	30	11	TevSTIB805.10.15350
60S ribosomal protein L4	13	33	13	TevSTIB805.3.5330
40S ribosomal protein S3A, putative	12	28	12	TevSTIB805.10.4180
40S ribosomal protein S4, putative	13	30	13	TevSTIB805.11_01.3720
60S ribosomal protein L10a	10	27	10	TevSTIB805.10.14150
40S ribosomal protein S24E, putative	13	29	13	TevSTIB805.10.7800
paraflagellar rod component, putative	17	27	17	TevSTIB805.8.6980
DHH1	15	26	15	TevSTIB805.10.4260
eukaryotic translation initiation factor 3 subunit 8	10	26	19	TevSTIB805.10.8760
unspecified product	11	29	9	TevSTIB805.11_01.11720
75 kDa invariant surface glycoprotein	12	25	7	TevSTIB805.5.350
ribosomal protein L3, putative	22	24	22	TevSTIB805.4.1860
elongation factor 2	14	19	14	TevSTIB805.10.4850
flagellar transport protein, putative	14	23	14	TevSTIB805.3.1070
intraflagellar transport protein IFT122, putative	12	23	5	TevSTIB805.5.3490
60S ribosomal protein L9, putative	9	23	6	TevSTIB805.10.1200
40S ribosomal protein S18, putative	13	22	11	TevSTIB805.10.5660
heat shock 70 kDa protein, putative	10	22	10	TevSTIB805.7.660
chaperone protein DNAj, putative	9	21	9	TevSTIB805.2.2870
glycerol-3-phosphate dehydrogenase [NAD], glycosomal	19	20	19	TevSTIB805.8.3630
t-complex protein 1 gamma subunit, putative	16	21	6	TevSTIB805.8.3230
retrotransposon hot spot (RHS) protein, putative	6	20	6	TevSTIB805.2.210
ribosomal protein L21E (60S), putative	12	20	12	TevSTIB805.11_01.630
60S ribosomal protein L13, putative	16	20	16	TevSTIB805.3.3390
glycerol kinase, glycosomal	11	20	11	TevSTIB805.9.9020
V-type ATPase, A subunit, putative	19	17	19	TevSTIB805.4.1130
coatomer alpha subunit, putative	7	19	1	TevSTIB805.4.470
40S ribosomal protein S9, putative	17	19	17	TevSTIB805.10.5950
hypothetical protein, conserved	22	15	22	TevSTIB805.7.3540
ATP-dependent DEAD/H RNA helicase, putative	14	18	4	TevSTIB805.3.2650
kinetoplastid membrane protein KMP-11	12	17	2	TevSTIB805.9.9950
40S ribosomal protein S3, putative	11	18	2	TevSTIB805.10.12110
75 kDa invariant surface glycoprotein, putative	14	16	9	TevSTIB805.5.340
NOT5 protein	10	17	10	TevSTIB805.3.1940
kinesin, putative	9	15	9	TevSTIB805.6.1820
hypothetical protein, conserved	13	19	13	TevSTIB805.7.2740
S-adenosylmethionine synthetase, putative	12	20	12	TevSTIB805.6.5010
hypothetical protein, conserved	13	18	13	TevSTIB805.6.4940
ATP-dependent phosphofructokinase	15	17	15	TevSTIB805.3.3350
glucose-regulated protein 78, luminal binding protein 1	9	19	9	TevSTIB805.11_01.7860
importin-alpha reexporter protein, putative	8	15	5	TevSTIB805.6.4910
60S ribosomal protein L23, putative	5	14	3	TevSTIB805.9.8140
14-3-3-like protein, putative	6	13	3	TevSTIB805.11_01.9820
antigenic protein, putative	3	17	3	TevSTIB805.4.2140

Figure 9. Analysis of proteins in TeEVs. (a) Western blot analysis of the purified TeEVs with anti-HSP70, anti-Aldolase, anti-KMP-11, and anti-EF-1α polyclonal antibodies. (b) Gene ontology analysis of proteins in EVs. (c) KEGG analysis of differential expressed genes.

induces BMDMs cytokines production remains unknown. In this study, we found that *T. evansi* could induce mouse BMDMs to secrete low-levels of IL-12p40, TNF-α and IL-6. Furthermore, *T. evansi* could induce the secretion of inflammatory cytokines via activating TLR2-ERK signaling pathway. However, no IFN-γ, IL-1β, IL-17A, IL-2, and IL-4 were detected. Previous studies have shown that IFN-γ can be rapidly produced by NK cells and NKT cells in the early stages during many pathogen infections [63–66]. CD4^{+} and CD8^{+} T cells are major producers of IFN-γ during *Plasmodium* infection [67]. In the present experiment, IFN-γ in serum might be secreted by other immune cells. There was no significant difference in IL-6 and TNF-α secretion between TLR2^{−/-} mouse BMDMs and WT mouse BMDMs after *T. evansi* stimulation. Surprisingly, IL-12p40 secretion in BMDMs of TLR2^{−/-} mice was significantly up-regulated compared with the BMDMs of WT mice. These results were consistent with the results of *in vivo* experiments. Furthermore, the phosphorylation of AKT induced by *T. evansi* was maintained for a long time and the secretions of IL-12p40, IL-6 and TNF-α were significantly enhanced in cells pretreated with AKT inhibitor. AKT inhibitor induced increased IL-12p40 in serum and helped to resist

T. evansi infection in mice. Similar studies found that *Giardia* inhibited the secretion of inflammatory cytokines through TLR2-AKT pathway [51] and *T. cruzi* infection in TLR2^{−/-} mice increased IL-12 secretion [68]. These results suggested that *T. evansi* could inhibit IL-12p40 secretion through the TLR2-AKT signaling pathway to escape host immune response.

Many parasites could secrete EVs via the endosomal sorting complexes required for transport (ESCRT) dependent mechanism, such as *T. cruzi* and *Neospora caninum* [33,69]. In addition, a new mechanism of EVs formation was found in *T. brucei*, which could extend nanotubes from the posterior end of the parasite and form EVs through nanotubes dissociation [36]. In this study, we isolated and identified TeEVs for the first time and found that the formation mechanism of TeEVs was consistent with that of *T. brucei*. Parasite-derived EVs could transfer their information to host cells by membrane fusion to play a vital role in the process of infecting the host and the host's immune response [28]. As an extracellular parasite, *T. brucei* could exchange information between the parasite and the host by secreting EVs, causing a series of immune responses in the host [36]. The EVs secreted by *N. caninum* could activate TLR2 of host macrophages and regulate the production of a series of cytokines
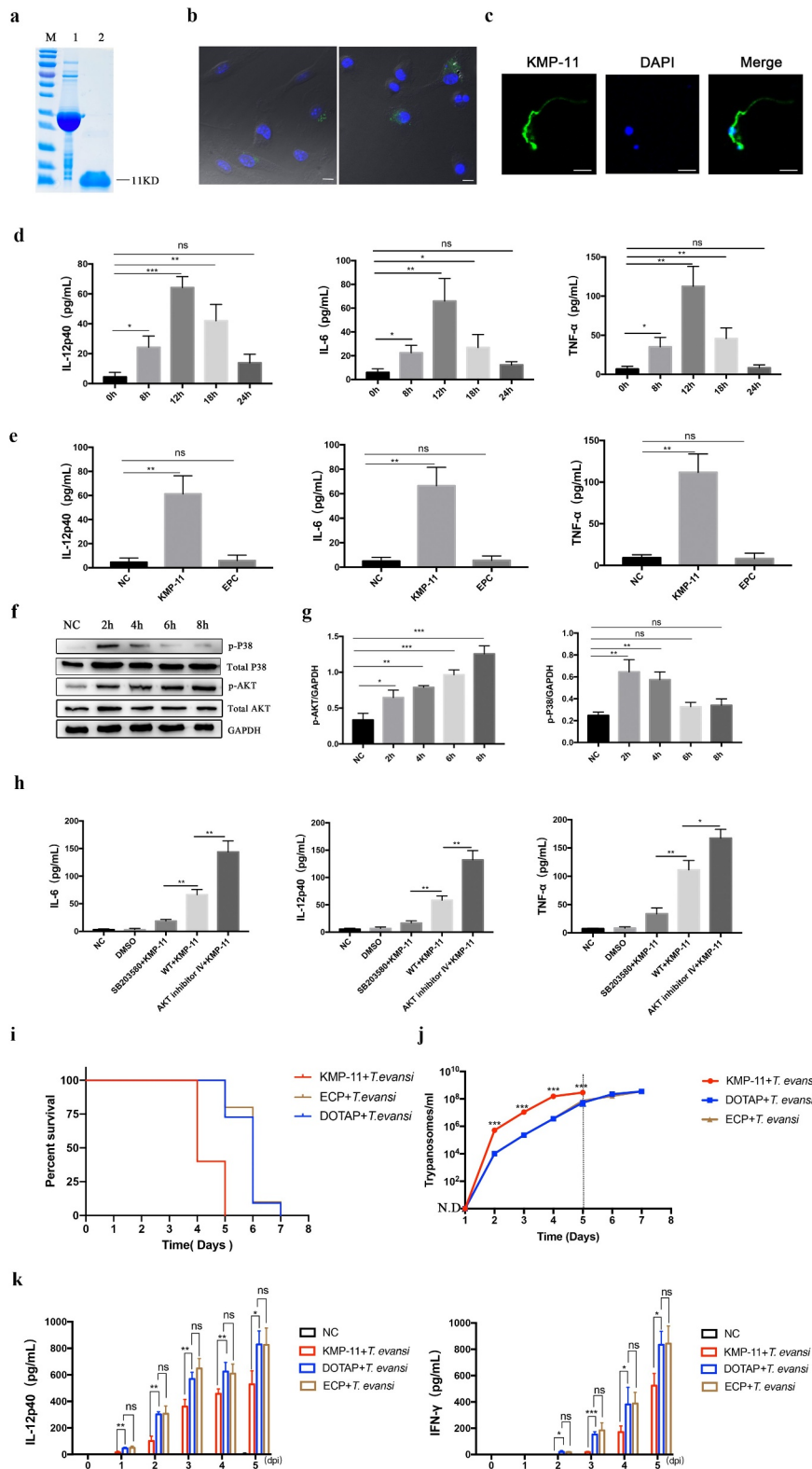
Figure 10. rTeKMP-11 activated AKT pathway to inhibit the secretion of inflammatory cytokines *in vitro* and promoted *T. evansi* proliferation *in vivo*. (a) Purified rTeKMP-11 protein. M, protein molecular markers. Lane 1, Purified rTeKMP-11 protein with vector tagged protein. Lane 2, rTeKMP-11 protein after removal of vector tagged protein. (b) BMDMs were stimulated with EVs (left) and rTeKMP-11 (right) for 2 h, the TeKMP-11 protein in BMDMs was detected by IFA and observed under confocal laser scanning. Green: TeKMP-11. Blue: nuclei. Scale bar = 5 μm. (c) The localization of TeKMP-11 protein in *T. evansi* was observed by laser confocal microscopy. Green: TeKMP-11. Blue: nuclei. Scale bar = 5 μm. (d) Secretion levels of IL-12p40, IL-6, and TNF-α in BMDMs

stimulated by 50 µg rTeKMP-11. (e) After stimulating with empty carrier protein (ECP), rTeKMP-11, and DOTAP for 12 h, the secretions of inflammatory cytokines were observed. (f, g) WT mouse BMDMs were stimulated with rTeKMP-11, Western blot and densitometric analysis were used to detect the phosphorylation levels of AKT and P38. (h) WT mouse BMDMs were stimulated with rTeKMP-11 after pretreated with SB203580 or AKT inhibitor IV for 1 h. The secretion levels of cytokines were measured by ELISA. (i-k) Mice (n = 10 mice per group) were injected intravenously (tail vein) with 50 µg rTeKMP-11 encapsulated in liposome, an equal volume of empty carrier protein or liposome for three consecutive days. (i) The death time was recorded daily. (j) Parasites load in peripheral blood was detected daily. (k) The production levels of IL-12p40, and IFN-γ in the serum were detected by ELISA. Bars represent the mean ± SEM for three experiments. ns, not significant; *, $P < 0.05$; **, $P < 0.01$; ***, $P < 0.001$, for the stimulated group versus the negative control group, or AKT/p38 inhibitor stimulation group versus WT stimulation group, or the rTeKMP-11 group versus the negative control group.

[33]. In this experiment, we investigated whether *T. evansi* could secrete EVs to regulate host immune response. TeEVs could activate the TLR2-AKT signaling pathway and inhibit IL-12p40, IL-6, and TNF-α *in vitro*. *In vivo*, we proved that EVs could inhibit the secretion of IL-12p40 and IFN-γ and increase parasite load in peripheral blood.

KMP-11 is a unique protein of kinetoplastid proteoa that is widely distributed on the surface of parasites. KMP-11 plays an important role in the cytoplasmic division of *T. brucei* [70]. As a virulence factor, KMP-11 induced increased IL-10 production, thus enhancing the infection of macrophages by *Leishmania* [71]. In this study, KMP-11 was identified as an important molecule of TeEVs to promote disease development in mice. rTeKMP-11 activated AKT and p38 signaling pathways to inhibit or promote the secretions of IL-12p40, IL-6, and TNF-α *in vitro*. EVs also carry a variety of proteins, including many virulence factors. The role of these EVs proteins in the interaction between *T. evansi* and host remains to be explored.

In conclusion, *T. evansi* could inhibit the productions of inflammatory cytokines via releasing TeEVs to activate TLR2-AKT signal pathways to survive successfully. TeKMP-11, a component of TeEVs, was involved in promoting *T. evansi* infection, which revealed a novel mechanism of *T. evansi* immune evasion.

Acknowledgments

Disclosure statement

The authors declare that they have no competing interests.

Funding

Data availability statement

The data that support the findings of this study are available from the corresponding author, Jianhua Li, upon reasonable request.

CRediT author statement

Ran Wei: Conceptualization, Original draft preparation, Methodology. **Xin Li**: Conceptualization, Methodology. **Xiaocen Wang**: Conceptualization, Original draft preparation. **Nan Zhang**: Conceptualization, Software. **Yuru Wang**: Software, Writing - Review & Editing. **Xichen Zhang**: Conceptualization, Data Curation. **Pengtao Gong**: Conceptualization, Data Curation. **Jianhua Li**: Supervision, Project administration.

Animal welfare statement

All experimental procedures strictly followed the guidelines provided by the administration of experimental animal affairs approved by state council of people's Republic of China and the animal welfare and research ethics committee of Jilin University (IACUC license No.: 201,701,009).

References

[1] Aregawi WG, Agga GE, Abdi RD, et al. Systematic review and meta-analysis on the global distribution, host range, and prevalence of *Trypanosoma evansi*. Parasit Vectors. 2019;12:67.

[2] Birhanu H, Roge S, Simon T, et al. Surra Sero K-SeT, a new immunochromatographic test for serodiagnosis of *Trypanosoma evansi* infection in domestic animals. Vet Parasitol. 2015;211(3–4):153–157.

[3] Desquesnes M, Dargantes A, Lai D-H, et al. *Trypanosoma evansi* and Surra: a review and perspectives on transmission, epidemiology and control, impact, and zoonotic aspects. Biomed Res Int. 2013;2013:20.

[4] Elhaig MM, Sallam NH. Molecular survey and characterization of *Trypanosoma evansi* in naturally infected

camels with suspicion of a Trypanozoon infection in horses by molecular detection in Egypt. Microb Pathog. 2018;123:201–205.

[5] Rashid I, Akbar H, Gharbi M, et al. First report of *Trypanosoma Evansi* Infection (SURRA) IN A PUMA (FELIS CONCOLOR) OF LAHORE ZOO, PAKISTAN. J Zoo Wildl Med. 2017;48(3):918–921.

[6] Herrera HM, Norek A, Freitas TP, et al. Domestic and wild mammals infection by *Trypanosoma evansi* in a pristine area of the Brazilian Pantanal region. Parasitol Res. 2005;96:121–126.

[7] Ereqat S, Nasereddin A, Al-Jawabreh A, et al. Prevalence of Trypanosoma evansi in livestock in Palestine. Parasit Vectors. 2020;13:21.

[8] Van Vinh Chau N, Buu Chau L, Desquesnes M, et al. A clinical and epidemiological investigation of the first reported human infection with the zoonotic parasite *Trypanosoma evansi* in Southeast Asia. Clin Infect Dis. 2016;62:1002–1008.

[9] Joshi PP, Shegokar VR, Powar RM, et al. Human trypanosomiasis caused by *Trypanosoma evansi* in India: the first case report. Am J Trop Med Hyg. 2005;73:491–495.

[10] Misra KK, Roy S, Choudhury A. Biology of *Trypanosoma (Trypanozoon) evansi* in experimental heterologous mammalian hosts. J Parasit Dis. 2016;40 (3):1047–1061.

[11] Kurup S, Tewari A. Induction of protective immune response in mice by a DNA vaccine encoding *Trypanosoma evansi* beta tubulin gene. Vet Parasitol. 2012;187(1–2):9–16.

[12] Faccio L, Da Silva AS, Gressler LT, et al. Susceptibility of Brazilian isolates of *Trypanosoma evansi* to suramin sodium: test in experimentally infected mice. Exp Parasitol. 2013;134(3):309–312.

[13] Gourbal B, Pinaud S, Beckers GJM, et al. Innate immune memory: an evolutionary perspective. Immunol Rev. 2018;283(1):21–40.

[14] Kawai T, Akira S. Pathogen recognition with Toll-like receptors. Curr Opin Immunol. 2005;17 (4):338–344.

[15] Janeway CA Jr., Medzhitov R. Innate Immune Recognition. Annu Rev Immunol. 2002;20(1):197–216.

[16] Akira S, Takeda K. Toll-like receptor signalling. Nat Rev Immunol. 2004;4(7):499–511.

[17] Souza COS, Gardinassi LG, Rodrigues V, et al. Monocyte and Macrophage-Mediated Pathology and protective immunity during schistosomiasis. Front Microbiol. 2020;11:1973.

[18] Oliveira AC, Peixoto JR, de Arruda LB, et al. Expression of functional TLR4 confers proinflammatory responsiveness to trypanosoma cruzi glycoinositolphospholipids and higher resistance to infection with T. cruzi. J Immunol. 2004;173(9):5688–5696.

[19] De Veer MJ, Curtis JM, Baldwin TM, et al. MyD88 is essential for clearance of *Leishmania major*: possible role for lipophosphoglycan and Toll-like receptor 2 signaling. Eur J Immunol. 2003;33(10):2822–2831.

[20] Srivastava S, Pandey SP, Jha MK, et al. *Leishmania* expressed lipophosphoglycan interacts with Toll-like receptor (TLR)-2 to decrease TLR-9 expression and reduce anti-*Leishmania*l responses. Clin Exp Immunol. 2013;172(3):403–409.

[21] Campos MA, Closel M, Valente EP, et al. Impaired production of proinflammatory cytokines and host resistance to acute infection with *Trypanosoma cruzi* in mice lacking functional myeloid differentiation factor 88. J Immunol. 2004;172(3):1711–1718.

[22] Ives A, Ronet C, Prevel F, et al. *Leishmania* RNA virus controls the severity of mucocutaneous leishmaniasis. Science. 2011;331(6018):775–778.

[23] Zaborowski MP, Balaj L, Breakefield XO, et al. Extracellular vesicles: composition, biological relevance, and methods of study. Bioscience. 2015;65 (8):783–797.

[24] Nowacki FC, Swain MT, Klychnikov OI, et al. Protein and small non-coding RNA-enriched extracellular vesicles are released by the pathogenic blood fluke *Schistosoma mansoni*. J Extracell Vesicles. 2015;4 (1):28665.

[25] Schorey JS, Cheng Y, Singh PP, et al. Exosomes and other extracellular vesicles in host-pathogen interactions. EMBO Rep. 2015;16(1):24–43.

[26] Bose S, Aggarwal S, Singh DV, et al. Extracellular vesicles: an emerging platform in gram-positive bacteria. Microb Cell. 2020;7(12):312–322.

[27] Rodrigues ML, Nakayasu ES, Oliveira DL, et al. Extracellular vesicles produced by *Cryptococcus neoformans* contain protein components associated with virulence. Eukaryot Cell. 2008;7(1):58–67.

[28] Szempruch AJ, Dennison L, Kieft R, et al. Sending a message: extracellular vesicles of pathogenic protozoan parasites. Nature Rev Microbiol. 2016;14 (11):669–675.

[29] Coakley G, Maizels RM, Buck AH. Exosomes and other extracellular vesicles: the new communicators in parasite infections. Trends Parasitol. 2015;31(10):477–489.

[30] Atayde VD, da Silva Lira Filho A, Chaparro V, et al. Exploitation of the Leishmania exosomal pathway by Leishmania RNA virus 1. Nat Microbiol. 2019;4 (4):714–723.

[31] Martin-Jaular L, Nakayasu ES, Ferrer M, et al. Exosomes from *Plasmodium yoelii*-infected reticulocytes protect mice from lethal infections. PLoS One. 2011;6(10):e26588.

[32] Twu O, de Miguel N, Lustig G, et al. *Trichomonas vaginalis* exosomes deliver cargo to host cells and mediate host□parasite interactions. PLoS Pathog. 2013;9(7):e1003482.

[33] Li S, Gong PT, Tai LX, et al. Extracellular vesicles secreted by *Neospora caninum* are recognized by toll-like receptor 2 and modulate host cell innate immunity through the MAPK Signaling Pathway. Front Immunol. 2018;9:1633.

[34] Tavares KC, Da Silva AS, Wolkmer P, et al. Cryopreservation of *Trypanosoma evansi* after DEAE-cellulose purification: evaluation of infective parameters. Res Vet Sci. 2011;90(2):257–259.

[35] Pineda-Torra I, Gage M, De Juan A, et al. Isolation, culture, and polarization of murine bone

marrow-derived and peritoneal macrophages. Methods Mol Biol. 2015;1339:101–109.

[36] Szempruch AJ, Sykes SE, Kieft R, et al. Extracellular vesicles from *Trypanosoma brucei* mediate virulence factor transfer and cause host anemia. Cell. 2016;164 (1–2):246–257.

[37] Aida Y, Pabst MJ. Removal of endotoxin from protein solutions by phase separation using Triton X-114. J Immunol Methods. 1990;132(2):191–195.

[38] Cheng Y, Ren X, Zhang Y, et al. eEF-2 kinase dictates cross-talk between autophagy and apoptosis induced by Akt inhibition, thereby modulating cytotoxicity of novel Akt inhibitor MK-2206. Cancer Res. 2011;71 (7):2654–2663.

[39] Aliberti JC, Cardoso MA, Martins GA, et al. Interleukin-12 mediates resistance to *Trypanosoma cruzi* in mice and is produced by murine macrophages in response to live trypomastigotes. Infect Immun. 1996;64(6):1961–1967.

[40] Wu H, Liu G, Shi M. Interferon Gamma in African trypanosome infections: friends or foes? Front Immunol. 2017;8:1105.

[41] Vincendeau P, Bouteille B. Immunology and immuno-pathology of African trypanosomiasis. An Acad Bras Cienc. 2006;78(4):645–665.

[42] Crawford AC, Lehtovirta-Morley LE, Alamir O, et al. Biphasic zinc compartmentalisation in a human fungal pathogen. PLoS Pathog. 2018;14(5):e1007013.

[43] Taylor JE, Rudenko G. Switching trypanosome coats: what's in the wardrobe? Trends Genet. 2006;22 (11):614–620.

[44] Tabel H, Wei G, Shi M. T cells and immunopathogenesis of experimental African trypanosomiasis. Immunol Rev. 2008;225(1):128–139.

[45] Stijlemans B, Caljon G, Van Den Abbeele J, et al. Immune Evasion Strategies of *Trypanosoma brucei* within the mammalian host: progression to pathogenicity. Front Immunol. 2016;7. DOI:10.3389/fimmu.2016.00233

[46] Magez S, Torres JEP, Obishakin E, et al. Infections with extracellular trypanosomes require control by efficient innate immune mechanisms and can result in the destruction of the mammalian humoral immune system. Front Immunol. 2020;11. DOI:10.3389/fimmu.2020.00382

[47] Kuriakose S, Onyilagha C, Singh R, et al. TLR-2 and MyD88-Dependent activation of MAPK and STAT proteins regulates proinflammatory cytokine response and immunity to experimental *Trypanosoma congolense* Infection. Front Immunol. 2019;10. DOI:10.3389/fimmu.2019.02673

[48] Zheng H, Tan ZP, Zhou TL, et al. The TLR2 is activated by sporozoites and suppresses intrahepatic rodent malaria parasite development. Sci Rep. 2015;5 (1). DOI:10.1038/srep18239

[49] Del Rio L, Butcher BA, Bennouna S, et al. *Toxoplasma gondii* triggers myeloid differentiation factor 88-Dependent IL-12 and Chemokine Ligand 2 (Monocyte Chemoattractant Protein 1) responses using distinct parasite molecules and host receptors. J Iimmunol. 2004;172(11):6954–6960.

[50] Muraille E, De Trez C, Brait M, et al. Genetically resistant mice lacking MyD88-Adapter protein display a high susceptibility to *Leishmania major* Infection associated with a Polarized Th2 response. J Iimmunol. 2003;170(8):4237–4241.

[51] Li X, Zhang X, Gong P, et al. TLR2$^{-/-}$ mice display decreased severity of giardiasis via enhanced proinflammatory cytokines production dependent on AKT signal pathway. Front Immunol. 2017;8. DOI:10.3389/fimmu.2017.01186

[52] Guerra CS, Silva RM, Carvalho LO, et al. Histopathological analysis of initial cellular response in TLR-2 deficient mice experimentally infected by *Leishmania (L.) amazonensis*. Int J Exp Pathol. 2010;91(5):451–459.

[53] Tarleton RL. Immune system recognition of *Trypanosoma cruzi*. Curr Opin Immunol. 2007;19 (4):430–434.

[54] Hunter CA, Slifer T, Araujo F. Interleukin-12-mediated resistance to *Trypanosoma cruzi* is dependent on tumor necrosis factor alpha and gamma interferon. Infect Immun. 1996;64(7):2381–2386.

[55] Barkhuizen M, Magez S, Atkinson RA, et al. Interleukin-12p70-dependent interferon- gamma production is crucial for resistance in African trypanosomiasis. J Infect Dis. 2007;196:1253–1260.

[56] Paim FC, Duarte MM, Costa MM, et al. Cytokines in rats experimentally infected with *Trypanosoma evansi*. Exp Parasitol. 2011;128:365–370.

[57] Kaushik RS, Uzonna JE, Zhang Y, et al. Innate resistance to experimental African trypanosomiasis: differences in cytokine (TNF-alpha, IL-6, IL-10 and IL-12) production by bone marrow-derived macrophages from resistant and susceptible mice. Cytokine. 2000;12:1024–1034.

[58] Truyens C, Torrico F, Angelo-Barrios A, et al. The cachexia associated with *Trypanosoma cruzi* acute infection in mice is attenuated by anti-TNF-alpha, but not by anti-IL-6 or anti-IFN-gamma antibodies. Parasite Immunol. 1995;17:561–568.

[59] Colineau L, Clos J, Moon KM, et al. *Leishmania donovani* chaperonin 10 regulates parasite internalization and intracellular survival in human macrophages. Med Microbiol Immunol. 2017;206:235–257.

[60] Dos-Santos AL, Carvalho-Kelly LF, Dick CF, et al. Innate immunomodulation to trypanosomatid parasite infections. Exp Parasitol. 2016;167:67–75.

[61] Stijlemans B, De Baetselier P, Magez S, et al. African trypanosomiasis-associated anemia: the contribution of the interplay between parasites and the mononuclear phagocyte system. Front Immunol. 2018;9:218.

[62] Mekata H, Konnai S, Mingala CN, et al. Kinetics of regulatory dendritic cells in inflammatory responses during Trypanosoma evansi infection. Parasite Immunol. 2012;34:318–329.

[63] Farrar MA, Schreiber RD. The molecular cell biology of interferon-gamma and its receptor. Annu Rev Immunol. 1993;11:571–611.

[64] Schroder K, Hertzog PJ, Ravasi T, et al. Interferon-gamma: an overview of signals, mechanisms and functions. J Leukoc Biol. 2004;75:163–189.

[65] Bafica A, Santiago HC, Goldszmid R, et al. Cutting edge: TLR9 and TLR2 signaling together account for MyD88-dependent control of parasitemia in *Trypanosoma cruzi* infection. J Immunol. 2006;177:3515–3519.

[66] Da Silva HB, Fonseca R, Alvarez JM, et al. IFN-gamma priming effects on the maintenance of effector memory CD4(+) T Cells and on phagocyte function: evidences from infectious diseases. J Immunol Res. 2015. DOI:10.1155/2015/202816

[67] Inoue S, Niikura M, Mineo S, et al. Roles of IFN-gamma and gammadelta T Cells in Protective immunity against blood-stage malaria. Front Immunol. 2013;4:258.

[68] Ropert C, Gazzinelli RT. Regulatory role of Toll-like receptor 2 during infection with *Trypanosoma cruzi*. J Endotoxin Res. 2004;10:425–430.

[69] Bayer-Santos E, Aguilar-Bonavides C, Rodrigues SP, et al. Proteomic analysis of trypanosoma cruzi secretome: characterization of two populations of extracellular vesicles and soluble proteins. J Proteome Res. 2013;12:883–897.

[70] Li Z, Wang CC. KMP-11, a basal body and flagellar protein, is required for cell division in *Trypanosoma brucei*. Eukaryot Cell. 2008;7:1941–1950.

[71] De Mendonca SC, Cysne-Finkelstein L, Matos DC. Kinetoplastid membrane protein-11 as a vaccine candidate and a virulence factor in *Leishmania*. Front Immunol. 2015;6:524.